

# Production and Decay of Di-photon Resonance at Future $e^+e^-$ Colliders

Hayato Ito and Takeo Moroi

*Department of Physics, University of Tokyo, Tokyo 113-0033, Japan*

## Abstract

Motivated by the ATLAS and CMS announcements of the excesses of di-photon events, we discuss the production and decay processes of di-photon resonance at future  $e^+e^-$  colliders. We assume that the excess of the di-photon events at the LHC is explained by a scalar resonance decaying into a pair of photons. In such a case, the scalar interacts with standard model gauge bosons and, consequently, the production of such a scalar is possible at the  $e^+e^-$  colliders. We study the production of the scalar resonance via the associated production with photon or  $Z$ , as well as via the vector-boson fusion, and calculate the cross sections of these processes. We also study the backgrounds, and discuss the detectability of the signals of scalar production with various decay processes of the scalar resonance. We also consider the case where the scalar resonance has an invisible decay mode, and study how the invisible decay can be observed at the  $e^+e^-$  colliders.

# 1 Introduction

High energy  $e^+e^-$  linear colliders, like International  $e^+e^-$  Linear Collider (ILC) [1–5] and Compact Linear Collider (CLIC) [6], are attractive candidates of energy frontier experiment in the future. The future  $e^+e^-$  colliders will not only study the detail of standard-model (SM) particles, particularly Higgs boson and top quark, but also provide important information about new physics at the electroweak scale (if it exists). For the  $e^+e^-$  linear collider experiments in the future, it is crucial to understand how and how well the information about various new physics models can be obtained there.

Notably, in December of 2015, both the ATLAS and CMS collaborations announced the excess in the di-photon invariant mass distribution [7, 8]. The ATLAS observed the excess with  $3.6\text{-}\sigma$  ( $2.0\text{-}\sigma$ ) local (global) significance at  $M_{\gamma\gamma} \simeq 750$  GeV (with  $M_{\gamma\gamma}$  being the di-photon invariant mass) for a narrow width case. Furthermore, the CMS result shows an excess with the local (global) significance of  $2.6\text{-}\sigma$  ( $1.2\text{-}\sigma$ ) at  $M_{\gamma\gamma} \simeq 760$  GeV. These signals may indicate the existence of a new scalar resonance with the mass of  $\sim 750$  GeV, although more data is needed to confirm or exclude such a possibility, (see, for example, [9–19]). If there exists such a resonance, its properties should be studied in detail by the future  $e^+e^-$  collider experiments [20–23].

Currently, the ILC is planned to be extendable up to  $\sqrt{s} \sim 1$  TeV (with  $\sqrt{s}$  being the center-of-mass (CM) energy of the collider). In addition, the energy of CLIC can be as high as a few TeV. With such CM energies, the resonance with its mass of  $\sim 750$  GeV is kinematically reachable. In particular, in some class of models, the resonance can be produced in association with neutral electroweak gauge bosons (i.e.,  $\gamma$  or  $Z$ ) and via the vector-boson fusion processes at the  $e^+e^-$  colliders. Once produced, the properties of the resonance may be studied with a high luminosity and a clean environment of the future  $e^+e^-$  colliders.

If there exists a new resonance, it is important to understand how it interacts with other fields. As mentioned above, one attractive explanation of the LHC di-photon excess is the existence of a scalar resonance with its mass of  $\sim 750$  GeV coupled to the standard-model (SM) gauge bosons. In addition, as well as the coupling to the gauge bosons, the scalar boson may also couple to other fields. For example, the scalar resonance may have a coupling to an invisible new particle which may be dark matter of the universe (see, for example, [10, 11]). Understanding of the properties of the scalar resonance will be a very important issue if it exists.

The purpose of this paper is to consider the production and the decay of the scalar boson (which we call  $\Phi$ ), which is responsible for the LHC di-photon excess, at the future  $e^+e^-$  colliders. We calculate the production cross section of such a scalar resonance at the  $e^+e^-$  colliders. We also estimate the number of backgrounds, and discuss the detectability of each decay mode of  $\Phi$ .

The organization of this paper is as follows. In Section 2, we summarize the model we consider. In Section 3, we discuss the production processes of  $\Phi$  at the  $e^+e^-$  colliders. In particular, we study the production of  $\Phi$  in association with  $\gamma$  or  $Z$ , and also the production

via the vector-boson fusion processes. In Section 4, we consider the detectability of the  $\Phi$  production signal in which  $\Phi$  decays into SM gauge bosons. Detectability of the invisible decay of  $\Phi$  is discussed in Section 5. Section 6 is devoted for conclusions and discussion.

## 2 Model

Let us first summarize the interaction of the new scalar boson of our interest. In order to make our discussion concrete, we assume that the scalar boson  $\Phi$  is pseudo-scalar, and that it has the following interaction

$$\mathcal{L}_{\text{eff}} = \frac{1}{2\Lambda_1}\Phi\epsilon^{\mu\nu\rho\sigma}\mathcal{B}_{\mu\nu}\mathcal{B}_{\rho\sigma} + \frac{1}{2\Lambda_2}\Phi\epsilon^{\mu\nu\rho\sigma}\mathcal{W}_{\mu\nu}^a\mathcal{W}_{\rho\sigma}^a + \frac{1}{2\Lambda_3}\Phi\epsilon^{\mu\nu\rho\sigma}\mathcal{G}_{\mu\nu}^A\mathcal{G}_{\rho\sigma}^A, \quad (2.1)$$

where  $\mathcal{B}_{\mu\nu}$ ,  $\mathcal{W}_{\mu\nu}^a$ , and  $\mathcal{G}_{\mu\nu}^A$  are field strength tensors for  $U(1)_Y$ ,  $SU(2)_L$ , and  $SU(3)_C$  gauge interactions, respectively, and the superscript  $a$  and  $A$  are indices of the adjoint representations of  $SU(2)_L$  and  $SU(3)_C$ , respectively. (Even if  $\Phi$  is a real scalar boson, the following results are almost unchanged.) The summations over the repeated indices are implicit. Because the interactions given in Eq. (2.1) are non-renormalizable, it is expected that there exists some dynamics which generates the interaction between  $\Phi$  and SM gauge bosons. We do not specify the dynamics behind the effective Lagrangian, and use Eq. (2.1) for our study.<sup>#1</sup>

With the above interaction terms, the partial decay rates of  $\Phi$  into the gauge bosons are given by

$$\Gamma(\Phi \rightarrow gg) = \frac{2m_\Phi^3}{\pi\Lambda_3^2}, \quad (2.2)$$

$$\Gamma(\Phi \rightarrow \gamma\gamma) = \frac{m_\Phi^3}{4\pi\Lambda_{\gamma\gamma}^2}, \quad (2.3)$$

$$\Gamma(\Phi \rightarrow \gamma Z) = \frac{m_\Phi^3}{8\pi\Lambda_{\gamma Z}^2} \left(1 - \frac{m_Z^2}{m_\Phi^2}\right)^3, \quad (2.4)$$

$$\Gamma(\Phi \rightarrow ZZ) = \frac{m_\Phi^3}{4\pi\Lambda_{ZZ}^2} \left(1 - \frac{4m_Z^2}{m_\Phi^2}\right)^{3/2}, \quad (2.5)$$

$$\Gamma(\Phi \rightarrow W^+W^-) = \frac{m_\Phi^3}{2\pi\Lambda_2^2} \left(1 - \frac{4m_W^2}{m_\Phi^2}\right)^{3/2}, \quad (2.6)$$

where  $m_\Phi$ ,  $m_Z$ , and  $m_W$  are the masses of  $\Phi$ ,  $Z$ , and  $W^\pm$ , respectively. For the definitions of  $\Lambda_{\gamma\gamma}$ ,  $\Lambda_{\gamma Z}$ , and  $\Lambda_{ZZ}$ , see Appendix. As we have mentioned, we also consider the case where  $\Phi$

---

<sup>#1</sup>If the energy of the collider becomes larger than the energy scale of the new physics responsible for the effective interaction, the calculation based on Eq. (2.1) may be inaccurate. We assume that it is not the case. In particular, if the scale of generating  $\mathcal{L}_{\text{eff}}$  is close to  $\sim \frac{1}{2}\sqrt{s}$ , on the contrary, momentum-dependent corrections to the effective Lagrangian can become sizable. Study of such an effect is interesting because it may reveal the dynamics behind the interaction of  $\Phi$  with the SM gauge bosons. Such an issue is, however, beyond the scope of our study, and we leave it for future study.

has an invisible decay mode. In such a case, we treat the invisible decay width  $\Gamma(\Phi \rightarrow \chi\chi)$  as a free parameter without specifying the interaction giving rise to such a decay. (Here and hereafter, the invisible particle is denoted as  $\chi$ .) One example is the interaction of the form  $\Phi\chi\chi$ , with which  $\chi$  is regarded as a gauge singlet Weyl fermion. For the total decay width  $\Gamma_\Phi$ , because  $\Phi$  may decay into particles other than the SM gauge bosons or the invisible particle,  $\Gamma_\Phi$  is regarded as a free parameter. In addition, we assume that  $\Gamma_\Phi \ll m_\Phi$  so that the narrow width approximation is applicable.

In the following, we consider two possible production processes at the LHC. One is the gluon-gluon fusion process, for which the LHC cross section (with the CM energy of 13 TeV) is estimated as

$$\sigma_{\text{LHC}}^{(gg)}(pp \rightarrow \Phi \rightarrow \gamma\gamma) \simeq 6.6 \text{ fb} \times \frac{\Gamma(\Phi \rightarrow gg)}{\Gamma_\Phi} \times \left[ \frac{\Gamma(\Phi \rightarrow \gamma\gamma)}{1 \text{ MeV}} \right], \quad (2.7)$$

and the other is photon-photon fusion process [24, 25], for which

$$\sigma_{\text{LHC}}^{(\gamma\gamma)}(pp \rightarrow \Phi \rightarrow \gamma\gamma) \simeq 24 \text{ fb} \times \left[ \frac{\Gamma_\Phi}{100 \text{ MeV}} \right]^{-1} \times \left[ \frac{\Gamma(\Phi \rightarrow \gamma\gamma)}{100 \text{ MeV}} \right]^2. \quad (2.8)$$

One should note that, with the di-photon production cross section at the LHC being fixed, a larger value of  $\Gamma(\Phi \rightarrow \gamma\gamma)$  is needed for the case of photon-photon fusion dominance compared to the gluon-gluon fusion dominance. This fact has an important implication to the  $e^+e^-$  colliders.

### 3 Production of $\Phi$ at the $e^+e^-$ Colliders

With the interaction given in Eq. (2.1), the  $\Phi$  production may occur at the  $e^+e^-$  colliders via several processes. We first consider the production processes in association with neutral electroweak gauge bosons:

- $e^+e^- \rightarrow \Phi\gamma$ ,
- $e^+e^- \rightarrow \Phi Z$ .

Feynman diagrams contributing to these processes are shown in Fig. 1. The analytic expressions of the cross sections of these processes are given in Appendix. In order to discuss the production process of  $\Phi$  at the  $e^+e^-$  colliders in the light of the LHC di-photon excess, it is convenient to parameterize the cross sections of these processes by using the LHC cross sections. Notably, the ratio  $\sigma(e^+e^- \rightarrow \Phi V)/\Gamma(\Phi \rightarrow \gamma\gamma)$  depends only on the ratio  $\Lambda_1/\Lambda_2$  (where  $V = \gamma$  or  $Z$ ). Then, using Eq. (2.7), one can see that the following relation holds:

$$\sigma(e^+e^- \rightarrow \Phi V) Br(\Phi \rightarrow F) \simeq \bar{\sigma}_{\Phi V}^{(gg)} \times \frac{\Gamma(\Phi \rightarrow F)}{\Gamma(\Phi \rightarrow gg)} \times \left[ \frac{\sigma_{\text{LHC}}^{(gg)}(pp \rightarrow \Phi \rightarrow \gamma\gamma)}{10 \text{ fb}} \right], \quad (3.1)$$

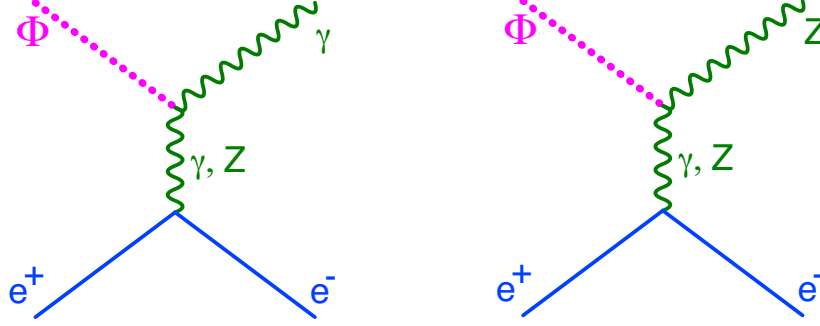


Figure 1: The Feynman diagrams for the processes  $e^+e^- \rightarrow \Phi\gamma$  and  $\Phi Z$ .

where  $\bar{\sigma}_{gg}^{(V)}$  depends only on the ratio  $\Lambda_1/\Lambda_2$  (as far as  $m_\Phi$  and  $\sqrt{s}$  are fixed). The above relation is useful when the LHC di-photon excess originates from the gluon-gluon fusion. In addition, using Eq. (2.8), we define  $\bar{\sigma}_{\Phi V}^{(\gamma\gamma)}$ , which is also a function of  $\Lambda_1/\Lambda_2$ , as

$$\sigma(e^+e^- \rightarrow \Phi V) Br(\Phi \rightarrow F) \simeq \bar{\sigma}_{\Phi V}^{(\gamma\gamma)} \times \frac{\Gamma(\Phi \rightarrow F)}{\Gamma(\Phi \rightarrow \gamma\gamma)} \times \left[ \frac{\sigma_{\text{LHC}}^{(\gamma\gamma)}(pp \rightarrow \Phi \rightarrow \gamma\gamma)}{10 \text{ fb}} \right]. \quad (3.2)$$

This expression can be used when the photon-photon fusion process is important at the LHC.

In Figs. 2 and 3, we plot  $\bar{\sigma}_{\Phi\gamma}^{(gg)}$  and  $\bar{\sigma}_{\Phi Z}^{(gg)}$  as functions of  $\Lambda_1/\Lambda_2$ , taking  $\sqrt{s} = 1, 1.5$ , and 2 TeV. (Here and hereafter, we take  $m_\Phi = 750$  GeV for our numerical calculations.) Here, the electron and positron beams are unpolarized, i.e.,  $P_{e-} = P_{e+} = 0$  (with  $P_{e-}$  and  $P_{e+}$  being the mean helicities of the initial-state electron and positron, respectively). Notice that the regions with too small or too large  $\Lambda_1/\Lambda_2$  are excluded by the 8 TeV run of the LHC. The most stringent bound comes from the negative searches for the resonance which decays into  $\gamma Z$ ; for example, taking  $\sigma(pp \rightarrow \Phi \rightarrow \gamma Z; 8 \text{ TeV}) < 11 \text{ fb}$  [17, 26] and the LHC cross section of the di-photon signal events to be 10 fb, only the region with  $-1 \lesssim \Lambda_1/\Lambda_2 \lesssim 6$  is allowed. In such a region,  $\bar{\sigma}_{\Phi\gamma}^{(gg)}$  and  $\bar{\sigma}_{\Phi Z}^{(gg)}$  are both of  $O(10^{-2} \text{ fb})$  or smaller with  $\sqrt{s} = 1 \text{ TeV}$ . With larger CM energy of  $\sim 1.5 - 2 \text{ TeV}$ , the cross sections may be as large as  $\sim 0.1 \text{ fb}$ .

Next, we consider the processes:

- $e^+e^- \rightarrow \Phi e^+e^-$ ,
- $e^+e^- \rightarrow \Phi \bar{\nu}_e \nu_e$ ,

to which the vector-boson fusion diagrams contribute (see Fig. 4). For these processes, we define

$$\sigma(e^+e^- \rightarrow \Phi \bar{l}l) Br(\Phi \rightarrow F) \simeq \bar{\sigma}_{\Phi \bar{l}l}^{(gg)} \times \frac{\Gamma(\Phi \rightarrow F)}{\Gamma(\Phi \rightarrow gg)} \times \left[ \frac{\sigma_{\text{LHC}}^{(gg)}(pp \rightarrow \Phi \rightarrow \gamma\gamma)}{10 \text{ fb}} \right], \quad (3.3)$$

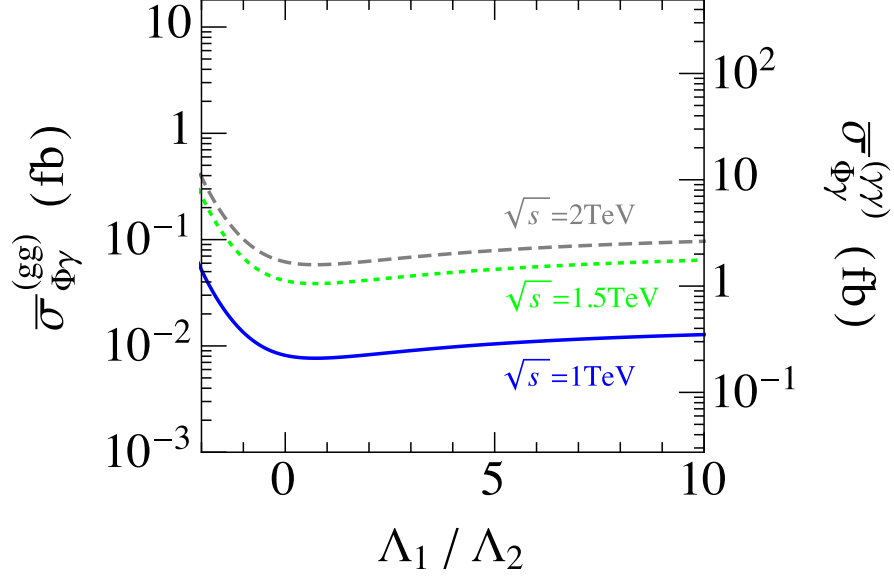


Figure 2:  $\bar{\sigma}_{\Phi\gamma}^{(gg)}$  as a function of  $\Lambda_1/\Lambda_2$ , with  $\sqrt{s} = 1, 1.5$ , and  $2$  TeV. Here we take  $P_{e-} = P_{e+} = 0$ . The right-horizontal axis shows the value of  $\bar{\sigma}_{\Phi\gamma}^{(\gamma\gamma)}$  using Eq. (3.9).

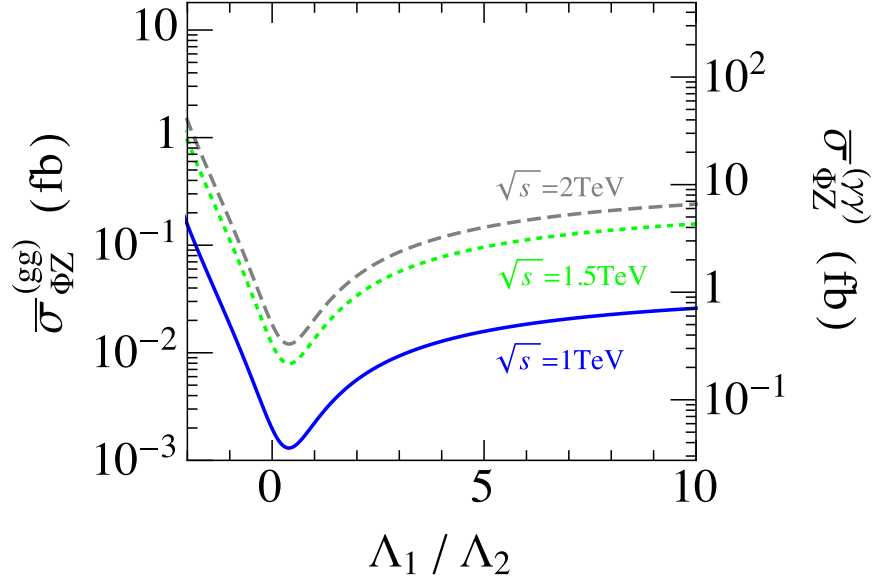


Figure 3:  $\bar{\sigma}_{\Phi Z}^{(gg)}$  as a function of  $\Lambda_1/\Lambda_2$ , with  $\sqrt{s} = 1, 1.5$ , and  $2$  TeV. Here we take  $P_{e-} = P_{e+} = 0$ . The right-horizontal axis shows the value of  $\bar{\sigma}_{\Phi Z}^{(\gamma\gamma)}$  using Eq. (3.9).

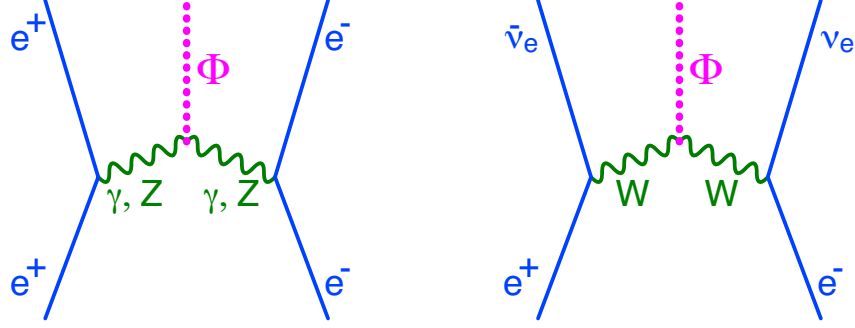


Figure 4: The vector-boson fusion diagrams contributing to the  $\Phi$  productions.

and

$$\sigma(e^+e^- \rightarrow \Phi \bar{l}l) Br(\Phi \rightarrow F) \simeq \bar{\sigma}_{\Phi \bar{l}l}^{(\gamma\gamma)} \times \frac{\Gamma(\Phi \rightarrow F)}{\Gamma(\Phi \rightarrow \gamma\gamma)} \times \left[ \frac{\sigma_{\text{LHC}}^{(\gamma\gamma)}(pp \rightarrow \Phi \rightarrow \gamma\gamma)}{10 \text{ fb}} \right], \quad (3.4)$$

with  $\bar{l}l = e^+e^-$  or  $\bar{\nu}_e\nu_e$ . Then,  $\bar{\sigma}_{\Phi \bar{l}l}^{(gg)}$  and  $\bar{\sigma}_{\Phi \bar{l}l}^{(\gamma\gamma)}$  depend only on  $\Lambda_1/\Lambda_2$ .

The cross section of the process  $e^+e^- \rightarrow \Phi e^+e^-$  is enhanced when the scattering angles of final-state  $e^+$  and  $e^-$  are both small. In such a case, the photon-photon fusion diagram shown in Fig. 4 is enhanced because the virtual photons are almost on-shell so that the denominators of the photon propagators become extremely small. Then, the photon-photon fusion diagram dominates over other diagrams which are less singular. In order to treat such an effect properly, we use the equivalent photon approximation [27]; for the final state of  $Fe^+e^-$ , we use

$$\sigma(e^+e^- \rightarrow Fe^+e^-) \simeq \int dx dx' f_\gamma(x; \theta_{e^+}^{(\min)}, \theta_{e^+}^{(\max)}) f_\gamma(x'; \theta_{e^-}^{(\min)}, \theta_{e^-}^{(\max)}) \sigma(\gamma\gamma \rightarrow F; sxx'), \quad (3.5)$$

where  $\theta_{e^\pm}^{(\min)}$  and  $\theta_{e^\pm}^{(\max)}$  are minimal and maximal scattering angles of  $e^\pm$ , respectively, and  $\sigma(\gamma\gamma \rightarrow F; E_{\text{cm}}^2)$  is the cross section of the unpolarized photon-photon collision process  $\gamma\gamma \rightarrow F$  with the center-of-mass energy  $E_{\text{cm}}$ . In addition,  $f_\gamma$  is the distribution function of the photon; for  $0 < x < 1$ ,  $f_\gamma$  is given by

$$f_\gamma(x, \theta^{(\min)}, \theta^{(\max)}) = \frac{\alpha}{2\pi} \left[ \frac{1 + (1-x)^2}{x} \ln \frac{|q^2|^{(\max)}}{|q^2|^{(\min)}} - 2m_e^2 x \frac{|q^2|^{(\max)} - |q^2|^{(\min)}}{|q^2|^{(\max)}|q^2|^{(\min)}} \right], \quad (3.6)$$

with  $m_e$  being the electron mass, and

$$|q^2|^{(\min, \max)} \equiv \frac{1}{2}s(1-x) \left[ 1 - \cos \theta^{(\min, \max)} + \frac{2x^2}{(1-x)^2} \frac{m_e^2}{s} \right], \quad (3.7)$$

while, otherwise,  $f_\gamma = 0$ . For the process of our interest, we obtain

$$\sigma(e^+e^- \rightarrow \Phi e^+e^-) \simeq \frac{8\pi^2 \Gamma(\Phi \rightarrow \gamma\gamma)}{sm_\Phi} \int \frac{dx}{x} f_\gamma(x; \theta_{e^+}^{(\min)}, \theta_{e^+}^{(\max)}) f_\gamma(m_\Phi^2/sx; \theta_{e^-}^{(\min)}, \theta_{e^-}^{(\max)}), \quad (3.8)$$

$\sqrt{s}$	Requirement 0	Requirement 1	Requirement 2
1 TeV	0.044 fb	0.015 fb	0.002 fb
1.5 TeV	0.18 fb	0.064 fb	0.007 fb
2 TeV	0.35 fb	0.12 fb	0.012 fb

Table 1:  $\bar{\sigma}_{\Phi e^+ e^-}^{(gg)}$  for  $\sqrt{s} = 1, 1.5$ , and 2 TeV, adopting the Requirement 0, 1 or 2.  $\bar{\sigma}_{\Phi e^+ e^-}^{(\gamma\gamma)}$  can be obtained by using Eq. (3.9).

where we used narrow width approximation.

The cross section of the process  $e^+e^- \rightarrow \Phi e^+e^-$  is logarithmically enhanced when  $\theta_{e^\pm}^{(\min)} \ll 1$ . For the study of the process  $e^+e^- \rightarrow \Phi e^+e^-$ , the energetic  $e^\pm$  in the forward direction may be used to eliminate the backgrounds. Since the ILC forward detectors are expected to cover up to  $O(1 - 10)$  mrad [5], we assume that energetic  $e^\pm$  with its energy  $E_{e^\pm}$  larger than 50 GeV can be identified with significant efficiency if the scattering angle  $\theta_{e^\pm}$  is larger than 10 mrad. We calculate the cross section, requiring that  $e^+$  and  $e^-$  are emitted to the forward directions. We consider the following three different requirements:

- Requirement 0: There is no  $e^\pm$  with  $\theta_{e^\pm} > 100$  mrad. (In this case, the scattering angles of  $e^\pm$  may be both so small that neither of  $e^\pm$  are detected.)
- Requirement 1: There is at least one  $e^\pm$  with  $E_{e^\pm} > 50$  GeV and  $\theta_{e^\pm} > 10$  mrad. In addition,  $\theta_{e^\pm} < 100$  mrad is required for both  $e^+$  and  $e^-$ .
- Requirement 2: The energies and the scattering angles of both  $e^+$  and  $e^-$  satisfy  $E_{e^\pm} > 50$  GeV and  $10 < \theta_{e^\pm} < 100$  mrad.

The results are shown in Table 1. (Notice that, with the equivalent photon approximation,  $\bar{\sigma}_{\Phi e^+ e^-}^{(gg)}$  is independent of  $\Lambda_1/\Lambda_2$ .) We have also checked that, if we require  $\theta_{e^\pm} > 20$  mrad for the detection instead of 10 mrad,  $\bar{\sigma}_{\Phi e^+ e^-}^{(gg)}$  decreases by  $\sim 30\%$  and  $\sim 50\%$  for the cases of Requirement 2 and 3, respectively.

For the process  $e^+e^- \rightarrow \Phi \bar{\nu}_e \nu_e$ , the  $W$ -boson fusion diagram contributes. Even though  $W$  is massive, such a diagram is enhanced when the neutrinos are emitted to the forward directions in the high energy limit. Thus, the cross section of such a process may potentially become larger than those for  $e^+e^- \rightarrow \Phi \bar{\nu}_\mu \nu_\mu$  and  $\Phi \bar{\nu}_\tau \nu_\tau$ , which are given by  $\sigma(e^+e^- \rightarrow \Phi Z)$  multiplied by branching ratios of  $Z$  into a neutrino pair. We also calculate  $\bar{\sigma}_{\Phi \bar{\nu}_e \nu_e}^{(gg)}$ , and the results are shown in Fig. 5. We found that  $\bar{\sigma}_{\Phi \bar{\nu}_e \nu_e}^{(gg)}$  is  $O(10^{-3})$  fb or smaller for  $\sqrt{s} = 1$  TeV.

So far, we have studied  $\bar{\sigma}_{\Phi X}^{(gg)}$  (with  $X = \gamma, Z, e^+e^-$ , or  $\bar{\nu}_e \nu_e$ ). For the calculations of  $\bar{\sigma}_{\Phi X}^{(\gamma\gamma)}$ , we can use the following proportionality:

$$\bar{\sigma}_{\Phi X}^{(\gamma\gamma)} \simeq 27 \bar{\sigma}_{\Phi X}^{(gg)}. \quad (3.9)$$



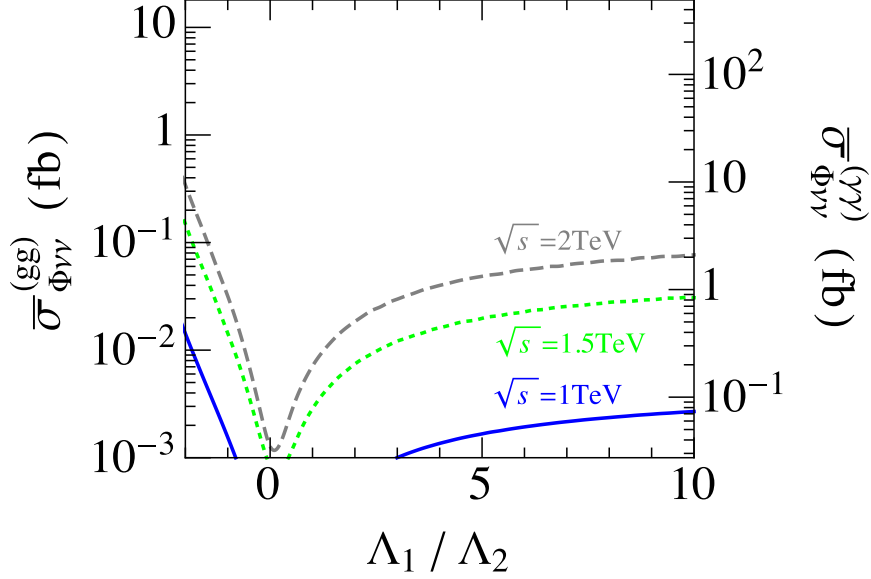


Figure 5:  $\bar{\sigma}_{\Phi\bar{\nu}_e\nu_e}^{(gg)}$  as a function of  $\Lambda_1/\Lambda_2$ , with  $\sqrt{s} = 1, 1.5$ , and  $2$  TeV. Here we take  $P_{e-} = P_{e+} = 0$ . The right-horizontal axis shows the value of  $\bar{\sigma}_{\Phi\bar{\nu}_e\nu_e}^{(\gamma\gamma)}$  using Eq. (3.9).

In particular, the values of  $\bar{\sigma}_{\Phi\gamma}^{(\gamma\gamma)}$ ,  $\bar{\sigma}_{\Phi Z}^{(\gamma\gamma)}$ , and  $\bar{\sigma}_{\Phi\bar{\nu}_e\nu_e}^{(\gamma\gamma)}$  are also shown in Figs. 2, 3, and 5, respectively. When the LHC di-photon excess at the LHC originates from the photon-photon fusion, the cross sections at the  $e^+e^-$  colliders become larger compared to the case of gluon-gluon fusion at the LHC. This is because, for the former case, a larger value of  $\Gamma(\Phi \rightarrow \gamma\gamma)$  needed (with the di-photon cross section at the LHC being fixed), resulting in stronger interaction of  $\Phi$  with electroweak gauge bosons.

## 4 Decay into SM Gauge Bosons

Now we are at the position to discuss the possibility of detecting the  $\Phi$  production at the future  $e^+e^-$  colliders. In this section, we consider the decay of  $\Phi$  into SM gauge bosons.

### 4.1 $e^+e^- \rightarrow \Phi\gamma$ and $e^+e^- \rightarrow \Phi Z$

We first consider the  $\Phi$  production in association with a SM gauge boson,  $e^+e^- \rightarrow \Phi V$ , followed by  $\Phi \rightarrow V'_1 V'_2$ , where  $V = \gamma$  or  $Z$ , and  $(V'_1, V'_2) = (g, g), (\gamma, \gamma), (\gamma, Z), (Z, Z)$ , or  $(W^+, W^-)$ . One characteristic feature of such an event is the existence of a monochromatic gauge boson. With the process  $e^+e^- \rightarrow \Phi V$ , the energy of the gauge boson  $V$  is given by

$$E_V^{(\text{sig})} = \frac{s - m_\Phi^2 + m_V^2}{2\sqrt{s}}, \quad (4.1)$$

where  $m_V$  is the mass of  $V$ . For the processes  $e^+e^- \rightarrow \Phi\gamma$  and  $\Phi Z$ ,  $E_\gamma^{(\text{sig})} = 219$  GeV and  $E_Z^{(\text{sig})} = 223$  GeV (859 GeV and 861 GeV) for  $\sqrt{s} = 1$  TeV (2 TeV), respectively. The kinematical cut based on  $E_V^{(\text{sig})}$  can be used to reduce backgrounds.

To estimate the number of backgrounds, we calculate the SM cross sections to produce  $\gamma$  or  $Z$  whose energy is close to  $E_V^{(\text{sig})}$  in association with two other gauge bosons (or energetic jets). For simplicity, we do not consider the decay of weak bosons nor the hadronization of partons. Then, in studying the backgrounds for the signal of  $e^+e^- \rightarrow \Phi\gamma$ , the following kinematical requirement is imposed:

- There is one photon whose energy satisfies  $|E_\gamma - E_\gamma^{(\text{sig})}| < 0.02E_\gamma^{(\text{sig})}$ , where  $E_\gamma$  is the energy of photon.

For the backgrounds for  $e^+e^- \rightarrow \Phi Z$ , we require:

- There is one  $Z$  whose energy satisfies  $|E_Z - E_Z^{(\text{sig})}| < 0.06E_Z^{(\text{sig})}$ , where  $E_Z$  is the energy of  $Z$ .

Notice that a very accurate measurement of the photon energy is expected at the ILC [5]; with the energy resolution of the electromagnetic calorimeter of the SiD detector, for example,  $\delta E/E = 0.17/\sqrt{E} \oplus 1$  % for electrons or photons. Furthermore, with the ILC detectors, the jet energy will be measured with the accuracy of 3 % or better for jet energies above 100 GeV. Thus, we take  $\sim 2\text{-}\sigma$  width of the detector resolution, assuming that we use the hadronic decay mode of  $Z$  for the latter process. In addition, we require that all the activities satisfy

- $|\eta| < 3$ ,

where  $\eta$  is the pseudorapidity.

For the signal events in which  $\Phi$  decays into a gluon pair, we expect that the dominant source of the backgrounds is  $e^+e^- \rightarrow q\bar{q}V$ , where  $q$  denotes light quarks; we calculate the SM cross sections of such processes with the cuts mentioned above. (In such a case,  $(V'_1, V'_2)$  should be understood as  $(q, \bar{q})$ .) For other cases, we calculate the SM cross section of the process  $e^+e^- \rightarrow V'_1V'_2V$ . The candidate of  $V$  (i.e., the gauge boson produced in association with  $\Phi$ ) is expected to be identified by using Eq. (4.1). In addition, we also assume that the final states with  $(V'_1, V'_2) = (Z, Z)$  and  $(W^+, W^-)$  can be distinguished with hadronically decaying  $Z$  and  $W^\pm$ , using the invariant masses of the decay products of  $V'_1$  and  $V'_2$  (which we denote  $m_{V'_1}$  and  $m_{V'_2}$ , respectively). Assuming 3 % uncertainty for the measurement of jet energies, the invariant masses of the  $Z$ - and  $W^\pm$ -systems are expected to be determined with the accuracy of  $\sim 4$  GeV, which is sizably smaller than the mass difference of  $Z$  and  $W^\pm$ . In particular, by studying  $m_{V'_1}$  and  $m_{V'_2}$  simultaneously, we expect that the  $(V'_1, V'_2) = (Z, Z)$  and  $(W^+, W^-)$  final states are distinguishable.<sup>#2</sup> The estimated numbers of backgrounds for the case of  $\sqrt{s} = 1$  and 2 TeV are summarized in Tables 2 and 3, respectively.

---

<sup>#2</sup>The authors thank K. Fujii for pointing this out.

Signal	$\gamma gg$	$Zgg$	$\gamma\gamma\gamma$	$\gamma\gamma Z$	$\gamma ZZ$	$ZZZ$	$\gamma W^+ W^-$	$ZW^+ W^-$
$e^+ e^- \rightarrow \Phi\gamma$	840	—	940	670	120	—	1200	—
$e^+ e^- \rightarrow \Phi Z$	—	900	—	810	550	120	—	3000

Table 2: The number of backgrounds for  $e^+ e^- \rightarrow \Phi\gamma$  and  $\Phi Z$ , with  $\sqrt{s} = 1$  TeV and  $L = 1 \text{ ab}^{-1}$ . Here we take  $P_{e^+} = P_{e^-} = 0$ .

Signal	$\gamma gg$	$Zgg$	$\gamma\gamma\gamma$	$\gamma\gamma Z$	$\gamma ZZ$	$ZZZ$	$\gamma W^+ W^-$	$ZW^+ W^-$
$e^+ e^- \rightarrow \Phi\gamma$	510	—	1500	890	130	—	1800	—
$e^+ e^- \rightarrow \Phi Z$	—	700	—	1800	1100	160	—	3800

Table 3: Same as Table 2, except for  $\sqrt{s} = 2$  TeV.

To discuss the detectability of each mode, we define

$$S_{VV_1'V_2'}/\sqrt{B_{VV_1'V_2'}} \equiv \frac{L\sigma(e^+e^- \rightarrow \Phi V)Br(\Phi \rightarrow V_1'V_2')\epsilon}{\sqrt{B_{VV_1'V_2'}}}, \quad (4.2)$$

where  $L$  is the luminosity,  $\epsilon$  is the efficiency due to the rapidity cut, and  $B_{VV_1'V_2'}$  is the number of backgrounds for the process  $e^+e^- \rightarrow \Phi V$ , followed by  $\Phi \rightarrow V_1'V_2'$ . Let us introduce

$$R_{EW} \equiv \frac{\Gamma(\Phi \rightarrow \gamma\gamma) + \Gamma(\Phi \rightarrow \gamma Z) + \Gamma(\Phi \rightarrow ZZ) + \Gamma(\Phi \rightarrow W^+W^-)}{\Gamma(\Phi \rightarrow gg)}, \quad (4.3)$$

which parametrizes the ratio of the gluon-gluon fusion and photon-photon fusion contributions to the LHC di-photon events; with sufficiently small (large) value of  $R_{EW}$ , the LHC di-photon excess is explained by the gluon-gluon (photon-photon) fusion process. Then, the ratio  $S_{VV_1'V_2'}/\sqrt{B_{VV_1'V_2'}}$  depends on the luminosity  $L$ ,  $\Lambda_1/\Lambda_2$ ,  $R_{EW}$ , and the LHC di-photon cross section  $\sigma_{LHC}(pp \rightarrow \Phi \rightarrow \gamma\gamma)$ , where

$$\sigma_{LHC}(pp \rightarrow \Phi \rightarrow \gamma\gamma) = \sigma_{LHC}^{(gg)}(pp \rightarrow \Phi \rightarrow \gamma\gamma) + \sigma_{LHC}^{(\gamma\gamma)}(pp \rightarrow \Phi \rightarrow \gamma\gamma). \quad (4.4)$$

For our numerical analysis, we take  $\sigma_{LHC}(pp \rightarrow \Phi \rightarrow \gamma\gamma) = 10 \text{ fb}$ . Using Eqs. (2.7) and (2.8), the gluon-gluon and photon-photon fusion contributions to the LHC di-photon cross section become comparable when  $\Gamma(\Phi \rightarrow \gamma\gamma) \simeq 27\Gamma(\Phi \rightarrow gg)$ .

First, let us consider the signal with  $(V_1', V_2') = (g, g)$ . The ratio  $S_{Vgg}/\sqrt{B_{Vgg}}$  is maximized when the LHC di-photon excess is explained by the gluon-gluon fusion process. In such a case,  $S_{Vgg}/\sqrt{B_{Vgg}}$  depends only on the ratio  $\Lambda_1/\Lambda_2$ ; with  $\sqrt{s} = 1$  TeV, it becomes larger than 5 when  $-4.9 < \Lambda_1/\Lambda_2 < -2.5$  and  $-8.2 < \Lambda_1/\Lambda_2 < -2.0$  for  $V = \gamma$  and  $V = Z$ , respectively. With  $\sigma_{LHC}(pp \rightarrow \Phi \rightarrow \gamma\gamma) = 10 \text{ fb}$ , however, such a value of  $\Lambda_1/\Lambda_2$  is already excluded by the 8 TeV run of the LHC, as we have mentioned in the previous section. Thus, with the  $\Phi$  production in association with  $\gamma$  or  $Z$ , we expect that the detection of  $gg$  final state is difficult.

Next, we consider the other decay modes of  $\Phi$ , i.e.,  $\Phi \rightarrow V'_1 V'_2$  with  $(V'_1, V'_2) = (\gamma, \gamma)$ ,  $(\gamma, Z)$ ,  $(Z, Z)$ , or  $(W^+, W^-)$ . As  $R_{EW}$  increases, the cross sections of the  $\Phi$  production with such decay processes increase. We estimate the minimal value of  $R_{EW}$  to see the signals, requiring  $S_{VV'_1 V'_2} / \sqrt{B_{VV'_1 V'_2}} > 5$ . The results are shown in Figs. 6 and 7 for  $\sqrt{s} = 1$  and 2 TeV, respectively. In the figures, we shaded the region where  $\sigma_{LHC}^{(\gamma\gamma)}(pp \rightarrow \Phi \rightarrow \gamma\gamma)$  becomes larger than  $\sigma_{LHC}^{(gg)}(pp \rightarrow \Phi \rightarrow \gamma\gamma)$ ; thus, in the shaded region, the LHC di-photon excess is explained by the photon-photon fusion process. We can see that the detection and the study of  $\Phi$  may be possible at the  $e^+e^-$  colliders with large enough  $R_{EW}$ . In particular, if the LHC di-photon excess is due to the photon-photon fusion, such a study seem possible even with  $\sqrt{s} = 1$  TeV and  $L = 1 \text{ ab}^{-1}$ .

## 4.2 $e^+e^- \rightarrow e^+e^-\Phi$

Next, we consider the process  $e^+e^- \rightarrow e^+e^-\Phi$ . The important feature of such a process is the existence of  $e^\pm$  which are (almost) parallel to the beam direction. Detection of such  $e^\pm$  may help to reduce backgrounds.

We consider the case where at least one of the final-state  $e^\pm$  is detectable. Then, as the signal, we require:

- Requirement 1 in the previous section: At least one  $e^\pm$  with  $E_{e^\pm} > 50 \text{ GeV}$  and  $\theta_{e^\pm} > 10 \text{ mrad}$ . In addition,  $\theta_{e^\pm} < 100 \text{ mrad}$  for both  $e^+$  and  $e^-$ .
- Candidates of  $V'_1$  and  $V'_2$ , which are the gauge bosons produced by the decay of  $\Phi$ . (Thus,  $(V'_1, V'_2) = (\gamma, \gamma)$ ,  $(g, g)$ ,  $(\gamma, Z)$ ,  $(Z, Z)$ , or  $(W^+, W^-)$ .)

In the following, we estimate the number of SM backgrounds for this type of events. In order to reduce the backgrounds, we impose kinematical selections based on the invariant mass of the  $V'_1 V'_2$  system (which is denoted as  $m_{V'_1 V'_2}$ ) and the pseudorapidities of  $V'_1$  and  $V'_2$ :

- $|m_{V'_1 V'_2} - m_\Phi| < 0.02m_\Phi$  for  $(V'_1, V'_2) = (\gamma, \gamma)$ , and  $|m_{V'_1 V'_2} - m_\Phi| < 0.06m_\Phi$  otherwise.
- $|\eta| < 1.47$  for  $V'_1$  and  $V'_2$ .

Notice that, for the signal events with  $\Phi \rightarrow gg$ , we expect that the dominant background is the process  $e^+e^- \rightarrow e^+e^-q\bar{q}$ . Thus, we also study the cross section of such a process.

Now we estimate the number of SM backgrounds. If there exists the process  $\gamma\gamma \rightarrow V'_1 V'_2$ , the cross section of  $e^+e^- \rightarrow e^+e^-V'_1 V'_2$  is logarithmically enhanced when the final-state  $e^+$  and  $e^-$  are both emitted to the forward directions. This is because diagrams containing  $n$  nearly on-shell photon propagators result in the cross section approximately proportional to  $\ln^n(|q^2|^{(\max)} / |q^2|^{(\min)})$ , as we discussed in the previous section (see Eq. (3.5)).

We first consider the cases where the final states are  $q\bar{q}$  or  $W^+W^-$ . In these cases, there exist tree-level processes  $\gamma\gamma \rightarrow q\bar{q}$  and  $W^+W^-$ . Therefore, for the backgrounds of these signal processes, diagrams with two nearly on-shell photon propagators are expected to be the most important. By using the equivalent photon approximation, we estimate the

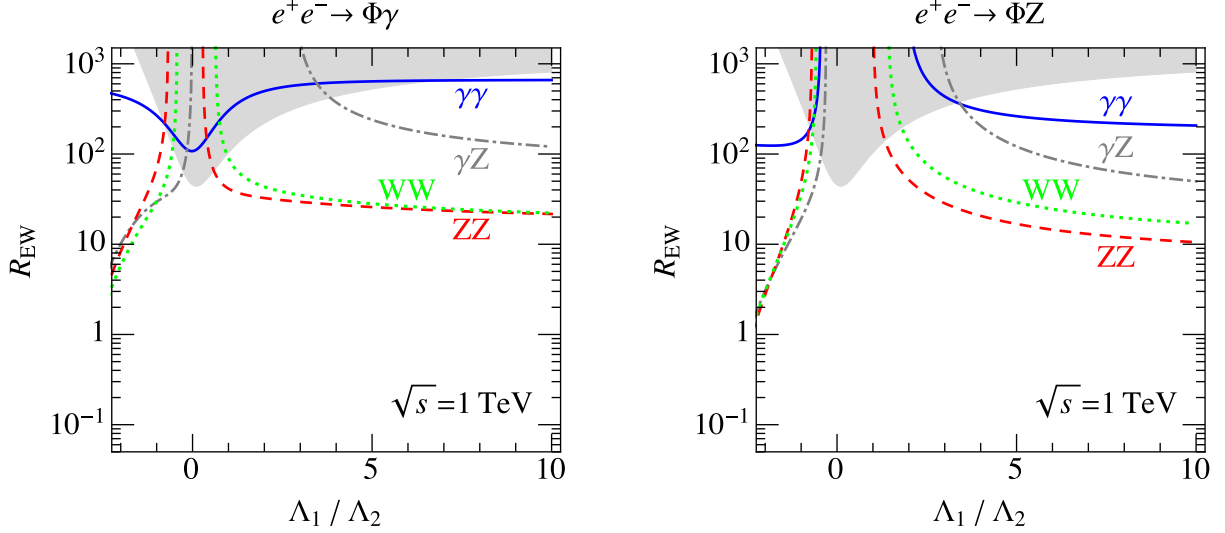


Figure 6: The minimal values of  $R_{EW}$  to realize  $S_{VV_1V_2'}/\sqrt{B_{VV_1V_2'}} > 5$  for  $V_1V_2' = \gamma\gamma$  (blue solid),  $\gamma Z$  (gray dot-dashed),  $ZZ$  (red dashed), and  $W^+W^-$  (green dotted) as function of the ratio  $\Lambda_1/\Lambda_2$ . Here we take  $\sqrt{s} = 1$  TeV,  $L = 1$  ab $^{-1}$ ,  $P_{e-} = P_{e+} = 0$ , and  $\sigma_{LHC}(pp \rightarrow \Phi \rightarrow \gamma\gamma) = 10$  fb. In the shaded region,  $\sigma_{LHC}^{(\gamma\gamma)}(pp \rightarrow \Phi \rightarrow \gamma\gamma)$  is larger than  $\sigma_{LHC}^{(gg)}(pp \rightarrow \Phi \rightarrow \gamma\gamma)$ .

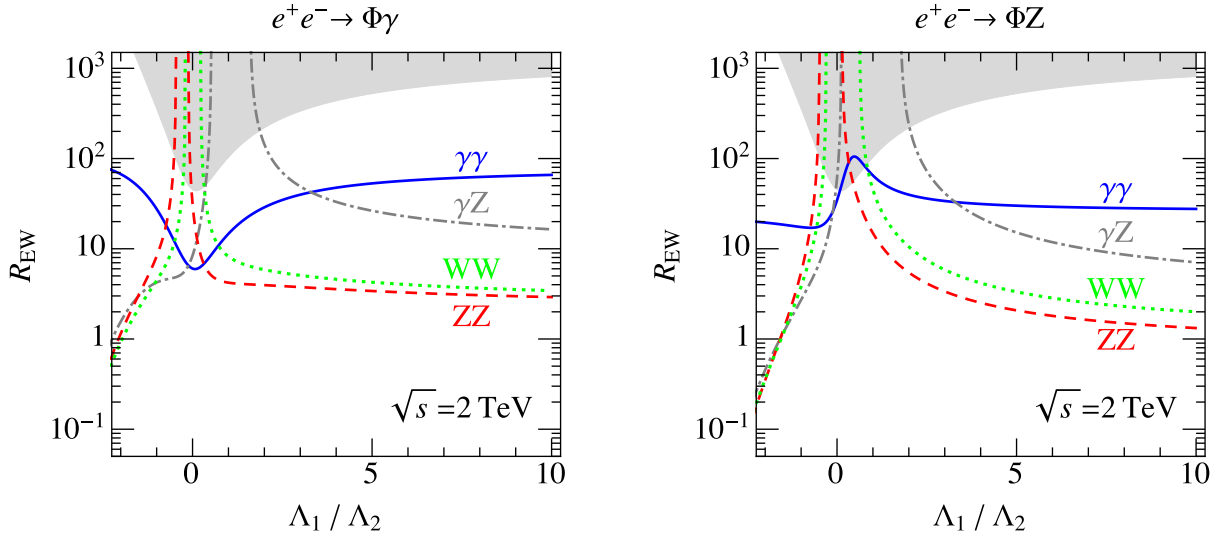


Figure 7: Same as Fig. 6, except for  $\sqrt{s} = 2$  TeV.

SM cross sections of the processes  $e^+e^- \rightarrow e^+e^-q\bar{q}$  and  $e^+e^-W^+W^-$ , imposing the above-mentioned kinematical selections. The expected numbers of backgrounds for  $L = 1 \text{ ab}^{-1}$  are 47 and 530 for  $(V'_1, V'_2) = (g, g)$  and  $(W^+, W^-)$ , respectively, taking  $\sqrt{s} = 1 \text{ TeV}$ . For  $\sqrt{s} = 2 \text{ TeV}$ , they are 250 and 2500, respectively. Since signal events with these final states suffer from large numbers of backgrounds compared to the other final states, as we will see below, we will not discuss further the detectability of these signal events.

We now consider the signals with  $\Phi \rightarrow V'_1V'_2$  with  $(V'_1, V'_2) = (\gamma, \gamma)$ ,  $(\gamma, Z)$ , and  $(Z, Z)$ . For these final states, the processes  $\gamma\gamma \rightarrow V'_1V'_2$  occur at the one-loop level, and are loop suppressed. Assuming that the one-loop processes with maximal logarithmic enhancements dominate the backgrounds, we estimate the number of backgrounds using the equivalent photon approximation; the cross sections of the processes  $\gamma\gamma \rightarrow \gamma\gamma$ ,  $\gamma Z$ , and  $ZZ$  can be found in [28–30]. Then, the numbers of backgrounds are estimated to be 0.2, 3.1, and 5.1 (1.0, 17, and 28) for  $(V'_1, V'_2) = (\gamma, \gamma)$ ,  $(\gamma, Z)$ , and  $(Z, Z)$ , respectively, taking  $L = 1 \text{ ab}^{-1}$  and  $\sqrt{s} = 1 \text{ TeV}$  (2 TeV).<sup>#3</sup>

With these background estimations, we calculate the minimal value of  $R_{\text{EW}}$  which realizes  $S_{eeV'_1V'_2}/\sqrt{B_{eeV'_1V'_2}} > 5$  for  $L = 1 \text{ ab}^{-1}$ , where

$$S_{eeV'_1V'_2} \equiv L\sigma(e^+e^- \rightarrow e^+e^-\Phi)Br(\Phi \rightarrow V'_1V'_2)\epsilon, \quad (4.5)$$

while  $B_{eeV'_1V'_2}$  is the number of backgrounds. If  $B_{eeV'_1V'_2}$  is less than 1, we require  $S_{eeV'_1V'_2} > 5$  instead. In Figs. 8 we show the minimal values of  $R_{\text{EW}}$  as functions of the ratio  $\Lambda_1/\Lambda_2$ . Comparing with Figs. 6 and 7, we can see that the process  $e^+e^- \rightarrow e^+e^-\Phi$  is easier to detect than  $e^+e^- \rightarrow \Phi V$  if  $\Phi$  decays into a pair of neutral electroweak gauge bosons.

## 5 Invisible Decay

In the previous section, we have considered the decay of  $\Phi$  into SM gauge bosons. Notably,  $\Phi$  may also couple to a new particle which is not in the particle content of the SM. In this section, we consider the case where  $\Phi$  couples to a particle which does not have a direct coupling to SM particles. In such a case,  $\Phi$  has an invisible decay mode; study of such a decay mode is an important step to understand the property of  $\Phi$ .

One possibility of detecting the invisible decay of  $\Phi$  at the  $e^+e^-$  colliders is to use the production process  $e^+e^- \rightarrow \Phi\gamma$  and  $\Phi Z$ , followed by the invisible decay of  $\Phi$ . In such processes, we observe energetic  $\gamma$  or the decay products of  $Z$  accompanied by large missing

---

<sup>#3</sup>In the tree-level diagrams contributing to the backgrounds of these processes, the number of nearly on-shell photon propagator is at most one. However, the tree level contributions are potentially important because there is no loop suppression. We have also studied the tree-level contributions by using `MadGraph5_aMC@NLO v2` [31] and `MadAnalysis` [32]. For  $10 < \theta_{e^\pm} < 100 \text{ mrad}$  for both  $e^+$  and  $e^-$ , we directly calculated the cross section of the process  $e^+e^- \rightarrow e^+e^-V'_1V'_2$ . For  $\theta_{e^+} < 10 \text{ mrad}$  and  $10 < \theta_{e^-} < 100 \text{ mrad}$ , (or for  $\theta_{e^-} < 10 \text{ mrad}$  and  $10 < \theta_{e^+} < 100 \text{ mrad}$ ), we adopted the equivalent photon approximation for the virtual photon emitted by  $e^+$  (or  $e^-$ ) and estimated the cross section. For both regions of the phase space, we found that the number of backgrounds with  $L = 1 \text{ ab}$  are much smaller than 1. Thus, we neglect the tree-level contributions.

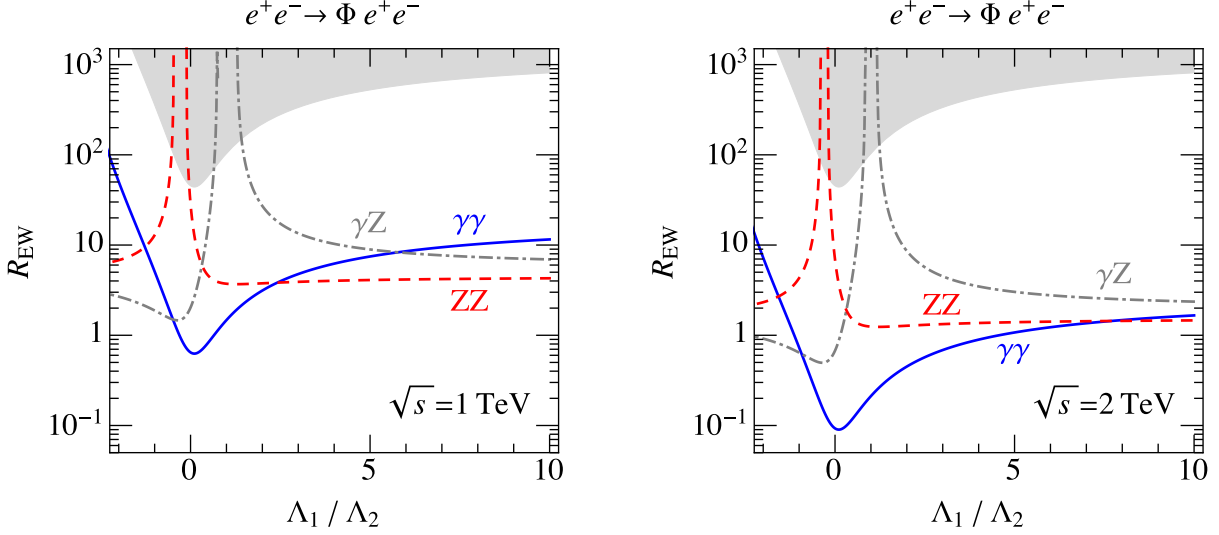


Figure 8: The minimal values of  $R_{EW}$  to realize  $S_{VV_1V_2'}/\sqrt{B_{VV_1V_2'}} > 5$  for  $V_1'V_2' = \gamma\gamma$  (blue solid),  $\gamma Z$  (gray dot-dashed), and  $ZZ$  (red dashed) as functions of the ratio  $\Lambda_1/\Lambda_2$ . In the shaded region,  $\sigma_{LHC}^{(\gamma\gamma)}(pp \rightarrow \Phi \rightarrow \gamma\gamma)$  is larger than  $\sigma_{LHC}^{(gg)}(pp \rightarrow \Phi \rightarrow \gamma\gamma)$ . Here we take  $\sqrt{s} = 1$  TeV (left) and 2 TeV (right),  $L = 1 \text{ ab}^{-1}$ , and  $P_{e-} = P_{e+} = 0$ .

momentum. In the signal event, the energy of the SM gauge boson is  $E_V^{(\text{sig})}$  given in Eq. (4.1). Thus, by selecting events with a single  $\gamma$  or  $Z$  candidate whose energy is close enough to  $E_V^{(\text{sig})}$ , we may be able to eliminate backgrounds to observe the invisible decay of  $\Phi$ .

For such a study, we estimate the number of backgrounds, applying cuts on the energy of SM gauge bosons. For the signal process  $e^+e^- \rightarrow \Phi\gamma$  with  $\Phi \rightarrow \chi\chi$ , we expect a single photon final state. As possible sources of backgrounds, we consider the following processes:

- (i)  $e^+e^- \rightarrow \gamma\bar{\nu}_l\nu_l$ ,
- (ii)  $e^+e^- \rightarrow \gamma\bar{\nu}_l\nu_l\bar{\nu}_{l'}\nu_{l'}$ ,

with  $l, l' = e, \mu$ , and  $\tau$ ; we calculate the cross sections of these processes requiring that the energy of  $\gamma$  is in the range of  $|E_\gamma - E_\gamma^{(\text{sig})}| < 0.02E_\gamma^{(\text{sig})}$ , and that  $|\eta| < 1$  for the final-state photon. For the signal process  $e^+e^- \rightarrow \Phi Z$  with  $\Phi \rightarrow \chi\chi$ , monochromatic  $Z$ -boson should be tagged to identify the signal. Here, we use the hadronic decay of  $Z$  because the hadronic branching ratio is larger than leptonic one. Then, we estimate the number of backgrounds by calculating the cross sections of the following processes:

- (iii)  $e^+e^- \rightarrow Z\bar{\nu}_l\nu_l$ ,
- (iv)  $e^+e^- \rightarrow Z\bar{\nu}_l\nu_l\bar{\nu}_{l'}\nu_{l'}$ ,

where we require that  $|E_Z - E_Z^{(\text{sig})}| < 0.06E_Z^{(\text{sig})}$ , and that  $|\eta| < 1$  for the  $Z$ -boson. We use **MadGraph5\_aMC@NLO** v2 [31] and **MadAnalysis** [32] to calculate the cross sections of the

	$\gamma + 2\nu$	$\gamma + 4\nu$	$Z + 2\nu$	$Z + 4\nu$
$\sqrt{s} = 1 \text{ TeV}$	560 (9100)	3.6 (37)	4800 (80000)	22 (330)
$\sqrt{s} = 2 \text{ TeV}$	78 (1100)	1.9 (9.3)	390 (6000)	5.1 (35)

Table 4: The number of backgrounds for  $e^+e^- \rightarrow \Phi\gamma$  and  $\Phi Z$  followed by  $\Phi \rightarrow \chi\chi$ , with  $\sqrt{s} = 1$  and 2 TeV, and  $L = 1 \text{ ab}^{-1}$ . Here we take  $P_{e+} = -0.3(+0.3)$  and  $P_{e-} = +0.8(-0.8)$  for the left (right) of each column.

background processes. The numbers of backgrounds of these processes with the luminosity of  $1 \text{ ab}^{-1}$  are summarized in Table 4, taking  $(P_{e+}, P_{e-}) = (-0.3, +0.8)$  and  $(+0.3, -0.8)$ . (We checked that one of these combinations of the helicities gives the best detectability, as far as  $|P_{e-}| = 0.8$  and  $|P_{e+}| = 0.3$ .)

The detectability of the invisible decay mode is studied by calculating the following quantity:

$$S_{V\chi\chi}/\sqrt{B_{V\chi\chi}} \equiv \frac{L\sigma(e^+e^- \rightarrow \Phi V)Br(\Phi \rightarrow \chi\chi)\epsilon}{\sqrt{B_{V\chi\chi}}}, \quad (5.1)$$

where  $B_{V\chi\chi}$  is the total number of the backgrounds for the process  $e^+e^- \rightarrow \Phi V$  followed by the invisible decay of  $\Phi$ . When the gluon-gluon fusion process dominates the LHC di-photon signal events,  $S_{V\chi\chi}/\sqrt{B_{V\chi\chi}}$  is proportional to the ratio of  $\Gamma(\Phi \rightarrow \chi\chi)/\Gamma(\Phi \rightarrow gg)$ , as can be understood from Eq. (3.1). On the other hand, it is proportional  $\Gamma(\Phi \rightarrow \chi\chi)/\Gamma(\Phi \rightarrow \gamma\gamma)$  for the case where the photon-photon fusion process is the origin of the LHC di-photon excess (see Eq. (3.2)). We have estimated the minimal values of these ratios as functions of  $\Lambda_1/\Lambda_2$  to observe the invisible decay of  $\Phi$  at the level of  $S_{V\chi\chi}/\sqrt{B_{V\chi\chi}} > 5$ . The results are shown in Figs. 9 and 10 for  $e^+e^- \rightarrow \Phi\gamma$  and  $\Phi Z$ , respectively. For the case where the di-photon excess at the LHC originates from the gluon-gluon fusion process, for example, the ILC with  $\sqrt{s} = 1 \text{ TeV}$  and  $L = 1 \text{ ab}^{-1}$  may observe the invisible decay of  $\Phi$  when  $\Gamma(\Phi \rightarrow \chi\chi)/\Gamma(\Phi \rightarrow gg) \sim O(10)$ .

## 6 Conclusions and Discussion

In this paper, we have studied the prospect of investigating the scalar boson  $\Phi$ , which is responsible for the di-photon excess observed at the LHC, using the future  $e^+e^-$  colliders. We have concentrated on the case where the LHC di-photon excess originates from the gluon-gluon and/or photon-photon fusion processes. We assumed that there exists a scalar boson  $\Phi$  with its mass of  $\sim 750 \text{ GeV}$ , and that  $\Phi$  directly couples to the SM gauge bosons via the dimension-five operators (see Eq. (2.1)).

We have studied the production process of  $\Phi$  in association with a SM gauge boson (i.e.,  $\gamma$  or  $Z$ ) and the production via the vector-boson fusion. We have calculated the cross sections of these processes. Then we have investigated the detectability of  $\Phi$  with estimating the SM



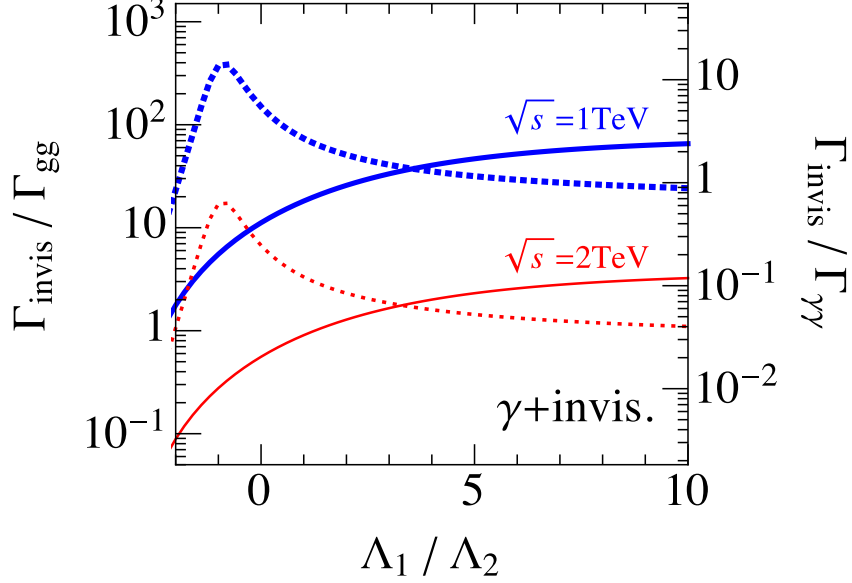


Figure 9: The minimal values of  $\Gamma(\Phi \rightarrow \chi\chi)/\Gamma(\Phi \rightarrow gg)$  (left horizontal axis, for the case where the LHC di-photon excess is due to the gluon-gluon fusion) and  $\Gamma(\Phi \rightarrow \chi\chi)/\Gamma(\Phi \rightarrow \gamma\gamma)$  (right horizontal axis, for the case where the LHC di-photon excess is due to the photon-photon fusion) to realize  $S_{\gamma\chi\chi}/\sqrt{B_{\gamma\chi\chi}} > 5$ , using the production process of  $e^+e^- \rightarrow \Phi\gamma$ . Here, we take  $\sqrt{s} = 1$  TeV (thick blue) and 2 TeV (thin red), and  $L = 1 \text{ ab}^{-1}$ . In addition, the helicities of  $e^\pm$  are  $(P_{e^+}, P_{e^-}) = (-0.3, -0.8)$  (solid) and  $(+0.3, -0.8)$  (dashed).

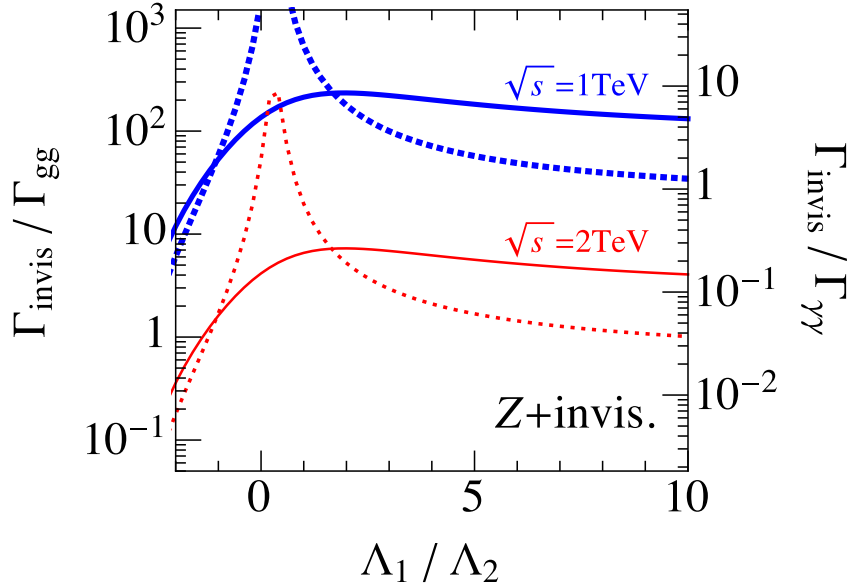


Figure 10: Same as Fig. 9, except for  $e^+e^- \rightarrow \Phi Z$ .

backgrounds. Detection of the decay mode of  $\Phi$  into the gluon pair seems difficult because the number of backgrounds is large. With the vector-boson fusion process, the decay of  $\Phi$  into the electroweak gauge bosons may be detected at the  $e^+e^-$  colliders if the decay width of such processes are of the same order of  $\Gamma(\Phi \rightarrow gg)$ , assuming that the LHC di-photon excess is due to the gluon-gluon fusion. In order to observe  $\Phi$ , the detection of energetic  $e^\pm$  in the forward directions is crucial to eliminate the backgrounds. We found that the observations of the associated production with  $\gamma$  or  $Z$  are more difficult because the numbers of backgrounds are order of magnitude larger. We have also studied the possibility of detecting the invisible decay of  $\Phi$  using the production process in association with  $\gamma$  or  $Z$ .

We comment on another possibility to study  $\Phi$  at the future  $e^+e^-$  facilities. Because  $\Phi$  couples directly to the photon pair, it can be produced at the photon-photon collider which is an important option of the future  $e^+e^-$  facilities. Indeed, in [20], it was shown that, even if the LHC di-photon excess originates from the gluon-gluon fusion, the  $\Phi$  production cross section at the photon-photon collider can be as large as  $\sim 100$  fb for  $\sqrt{s} \sim 1$  TeV, which is much larger than that with the  $e^+e^-$  collision. With such a large cross section, a significant number of  $\Phi$  will be available for its detailed study.

Based on our analysis, the expected number of  $\Phi$  production at the ILC is of  $O(10)$  with  $\sqrt{s} = 1$  TeV and  $L = 1$  ab $^{-1}$ , if the LHC di-photon excess is due to the gluon-gluon fusion and also if  $\Phi$  dominantly decays into the gluon pair. If the LHC di-photon excess is from the photon-photon fusion, the number of  $\Phi$  produced at the ILC becomes larger. In addition, even if the  $\Phi$  production at the LHC is dominated by the gluon-gluon fusion, the invisible decay of  $\Phi$  may be observed at the ILC if the invisible decay width is an order of magnitude larger than the decay width into the gluon pair. Thus, the ILC will provide interesting possibilities to study the properties of the di-photon resonance.

*Acknowledgment:* The authors are grateful to Y. Takaesu for the collaboration at the early stage of this project. They also thank K. Fujii and T. Tanabe for useful comments. The work of T.M. is supported by JSPS KAKENHI No. 26400239.

## Appendix: Cross Sections

In this Appendix, we give the expressions for the cross sections of the resonance production in association with SM gauge bosons. For the case with pseudo-scalar resonance, we adopt the interaction terms given in Eq. (2.1). For completeness, we also consider the case where the new scalar resonance is a scalar boson, for which the interaction terms are given by<sup>#4</sup>

$$\mathcal{L}_{\text{eff}} = \frac{1}{\Lambda_1} \Phi \mathcal{B}_{\mu\nu} \mathcal{B}_{\mu\nu} + \frac{1}{\Lambda_2} \Phi \mathcal{W}_{\mu\nu}^a \mathcal{W}_{\mu\nu}^a + \frac{1}{\Lambda_3} \Phi \mathcal{G}_{\mu\nu}^A \mathcal{G}_{\mu\nu}^A. \quad (\text{A.1})$$

The following formulae can be used for both pseudo-scalar and scalar cases.

---

<sup>#4</sup>For the notational simplicity, we use the same notation for the suppression scales of the dimension-five operators in the pseudo-scalar and scalar cases.

Then, denoting the angle between the beam axis and the direction of the  $\Phi$  in the CM frame as  $\theta$ , the differential cross sections of the  $\Phi$  production in association with a SM gauge boson with fully-polarized initial-state  $e^\pm$  is given by

$$\frac{d\sigma(e_R^+e_L^- \rightarrow \Phi V)}{d\cos\theta} = \frac{\beta}{32\pi} C_V^{(L)} [s^2\beta^2(1 + \cos^2\theta) + 8\xi_\Phi s m_V^2], \quad (\text{A.2})$$

with  $V = \gamma$  and  $Z$ ;  $d\sigma(e_L^+e_R^- \rightarrow \Phi V)/d\cos\theta$  can be obtained by exchanging  $L \leftrightarrow R$ , while  $\sigma(e_L^+e_L^- \rightarrow \Phi V) = \sigma(e_R^+e_R^- \rightarrow \Phi V) = 0$ . Here,  $\xi_\Phi = 0$  for the pseudo-scalar production processes, while  $\xi_\Phi = 1$  for the scalar production,  $m_V = 0$  and  $m_Z$  for  $V = \gamma$  and  $Z$ , respectively, and

$$\beta = \frac{1}{s} \sqrt{s^2 - 2(m_\Phi^2 + m_V^2)s + (m_\Phi^2 - m_V^2)^2}. \quad (\text{A.3})$$

In addition,

$$C_\gamma^{(L,R)} = \left[ \frac{2e}{\Lambda_{\gamma\gamma}s} - \frac{g_{Ze}^{(L,R)}}{\Lambda_{\gamma Z}(s - m_Z^2)} \right]^2, \quad (\text{A.4})$$

$$C_Z^{(L,R)} = \left[ \frac{e}{\Lambda_{\gamma Z}s} - \frac{2g_{Ze}^{(L,R)}}{\Lambda_{ZZ}(s - m_Z^2)} \right]^2, \quad (\text{A.5})$$

where

$$\Lambda_{\gamma\gamma}^{-1} \equiv \frac{g_1^2}{g_Z^2} \Lambda_2^{-1} + \frac{g_2^2}{g_Z^2} \Lambda_1^{-1}, \quad (\text{A.6})$$

$$\Lambda_{\gamma Z}^{-1} \equiv \frac{2g_1g_2}{g_Z^2} (\Lambda_2^{-1} - \Lambda_1^{-1}), \quad (\text{A.7})$$

$$\Lambda_{ZZ}^{-1} \equiv \frac{g_2^2}{g_Z^2} \Lambda_2^{-1} + \frac{g_1^2}{g_Z^2} \Lambda_1^{-1}, \quad (\text{A.8})$$

with  $g_1$  and  $g_2$  being the gauge coupling constants of  $U(1)_Y$  and  $SU(2)_L$ , respectively,  $g_Z \equiv \sqrt{g_1^2 + g_2^2}$ ,<sup>#5</sup> and

$$e = \frac{g_1g_2}{g_Z}, \quad g_{Ze}^{(L)} = \frac{g_1^2 - g_2^2}{2g_Z}, \quad g_{Ze}^{(R)} = \frac{g_1^2}{g_Z}. \quad (\text{A.9})$$

## References

- [1] T. Behnke *et al.*, arXiv:1306.6327 [physics.acc-ph];

---

<sup>#5</sup>In our numerical calculations, we use the gauge coupling constants at the renormalization scale of  $\mu = m_Z$ . For more accurate calculations, inclusion of the effects of renormalization group running of the gauge coupling constants are relevant.

- [2] H. Baer *et al.*, arXiv:1306.6352 [hep-ph];
- [3] C. Adolphsen *et al.*, arXiv:1306.6353 [physics.acc-ph];
- [4] C. Adolphsen *et al.*, arXiv:1306.6328 [physics.acc-ph];
- [5] T. Behnke *et al.*, arXiv:1306.6329 [physics.ins-det].
- [6] L. Linssen, A. Miyamoto, M. Stanitzki and H. Weerts, arXiv:1202.5940 [physics.ins-det].
- [7] The ATLAS Collaboration, ATLAS-CONF-2015-081 (2015).
- [8] The CMS Collaboration, CMS PAS EXO-15-004 (2015).
- [9] K. Harigaya and Y. Nomura, Phys. Lett. B **754** (2016) 151 [arXiv:1512.04850 [hep-ph]].
- [10] Y. Mambrini, G. Arcadi and A. Djouadi, Phys. Lett. B **755** (2016) 426 [arXiv:1512.04913 [hep-ph]].
- [11] M. Backovic, A. Mariotti and D. Redigolo, JHEP **1603** (2016) 157 [arXiv:1512.04917 [hep-ph]].
- [12] A. Angelescu, A. Djouadi and G. Moreau, Phys. Lett. B **756** (2016) 126 [arXiv:1512.04921 [hep-ph]].
- [13] Y. Nakai, R. Sato and K. Tobioka, arXiv:1512.04924 [hep-ph].
- [14] S. Knapen, T. Melia, M. Papucci and K. Zurek, arXiv:1512.04928 [hep-ph].
- [15] D. Buttazzo, A. Greljo and D. Marzocca, Eur. Phys. J. C **76** (2016) no.3, 116 [arXiv:1512.04929 [hep-ph]].
- [16] A. Pilaftsis, Phys. Rev. D **93** (2016) no.1, 015017 [arXiv:1512.04931 [hep-ph]].
- [17] R. Franceschini *et al.*, JHEP **1603** (2016) 144 [arXiv:1512.04933 [hep-ph]].
- [18] S. Di Chiara, L. Marzola and M. Raidal, arXiv:1512.04939 [hep-ph].
- [19] T. Higaki, K. S. Jeong, N. Kitajima and F. Takahashi, Phys. Lett. B **755** (2016) 13 [arXiv:1512.05295 [hep-ph]].
- [20] H. Ito, T. Moroi and Y. Takaesu, Phys. Lett. B **756** (2016) 147 [arXiv:1601.01144 [hep-ph]].
- [21] N. Sonmez, arXiv:1601.01837 [hep-ph].
- [22] A. Djouadi, J. Ellis, R. Godbole and J. Quevillon, JHEP **1603** (2016) 205 [arXiv:1601.03696 [hep-ph]].

- [23] M. He, X. G. He and Y. Tang, arXiv:1603.00287 [hep-ph].
- [24] C. Csaki, J. Hubisz and J. Terning, Phys. Rev. D **93** (2016) 035002 [arXiv:1512.05776 [hep-ph]].
- [25] C. Csaki, J. Hubisz, S. Lombardo and J. Terning, arXiv:1601.00638 [hep-ph].
- [26] G. Aad *et al.* [ATLAS Collaboration], Phys. Lett. B **738** (2014) 428 [arXiv:1407.8150 [hep-ex]].
- [27] V. M. Budnev, I. F. Ginzburg, G. V. Meledin and V. G. Serbo, Phys. Rept. **15** (1975) 181.
- [28] G. J. Gounaris, P. I. Porfyriadis and F. M. Renard, Eur. Phys. J. C **9** (1999) 673 [hep-ph/9902230].
- [29] G. J. Gounaris, J. Layssac, P. I. Porfyriadis and F. M. Renard, Eur. Phys. J. C **10** (1999) 499 [hep-ph/9904450].
- [30] G. J. Gounaris, J. Layssac, P. I. Porfyriadis and F. M. Renard, Eur. Phys. J. C **13** (2000) 79 [hep-ph/9909243].
- [31] J. Alwall *et al.*, JHEP **1407**, 079 (2014) [arXiv:1405.0301 [hep-ph]].
- [32] E. Conte, B. Fuks and G. Serret, Comput. Phys. Commun. **184**, 222 (2013) [arXiv:1206.1599 [hep-ph]].